Physics in Medicine & Biology

PAPER • OPEN ACCESS

Exploring the performance of a DOI-capable TOF-PET module using different SiPMs, customized and commercial readout electronics

To cite this article: Giulia Terragni *et al* 2025 *Phys. Med. Biol.* **70** 025015

IOP Publishing Phys. Med. Biol. 70 (2025) 025015 https://doi.org/10.1088/1361-6560/ada19a

Physics in Medicine & Biology

IPEM Institute of Physics and Engineering in Medicine

OPEN ACCESS

RECEIVED
8 July 2024

REVISED
19 November 2024

ACCEPTED FOR PUBLICATION
19 December 2024

PUBLISHED
17 January 2025

PAPER

Exploring the performance of a DOI-capable TOF-PET module using different SiPMs, customized and commercial readout electronics

Giulia Terragni[1,2,*], Vanessa Nadig[3], Elena Tribbia[1,4], Stefano di Gangi[4], Ekaterini Toumparidou[3], Thomas Meyer[1], Johann Marton[2], Volkmar Schulz[3,5,6,7], Stefan Gundacker[3,8], Marco Pizzichemi[1,4] and Etiennette Auffray[1]

[1] CERN, Geneva, Switzerland
[2] Technical University of Vienna, Vienna, Austria
[3] Department of Physics of Molecular Imaging Systems, RWTH Aachen University, Aachen, Germany
[4] University of Milano-Bicocca, Milan, Italy
[5] Hyperion Hybrid Imaging Systems GmbH, Aachen, Germany
[6] Physics Institute IIIB, RWTH Aachen University, Aachen, Germany
[7] Now at Institute of Imaging & Computer Vision, RWTH Aachen University, Aachen, Germany.
[8] Now at Institute of High Energy Physics, Austrian Academy of Sciences, Vienna, Austria.
[*] Author to whom any correspondence should be addressed.

E-mail: giulia.terragni@cern.ch

Keywords: time-of-flight PET, coincidence time resolution (CTR), depth-of-interaction (DOI), light-sharing, PETsys TOFPET2 ASIC, NINO chip

Abstract

Objective. Time resolution is crucial in positron emission tomography (PET) to enhance the signal-to-noise ratio and image quality. Moreover, high sensitivity requires long scintillators, which can cause distortions in the reconstructed images due to parallax effects. This study evaluates the performance of a time-of-flight (TOF)-PET module that makes use of a single-side readout of a 4×4 $3.1 \times 3.1 \times 15$ mm^3 LYSO:Ce matrix with an array of 4×4 silicon photomultipliers (SiPMs) and a light guide to extract high-resolution TOF and depth of interaction (DOI) information. *Approach.* This study assesses the performance of the detector prototype using the commercially available TOFPET2 ASIC and SiPMs from various producers. DOI and TOF performance are compared to results using custom-made NINO 32-chip based electronics. *Main results.* Using a Broadcom NUV-MT array, the detector module read out by the TOFPET2 ASIC demonstrates a DOI resolution of 2.6 ± 0.2 mm full width at half maximum (FWHM) and a coincidence time resolution (CTR) of 216 ± 6 ps FWHM. When read out using the NINO 32-chip based electronics, the same module achieves a DOI resolution of 2.5 ± 0.2 mm and a CTR of 170 ± 5 ps. *Significance.* The prototype module, read out by commercial electronics and using state-of-the-art SiPMs, achieves a DOI performance comparable to that obtained with custom-made electronics and a CTR of around 200 ps. This approach is scalable to thousands of channels, with only a deterioration in timing resolution compared to the custom-made electronics, which achieve a CTR of 140 ps using a standard non-DOI module.

1. Introduction

Positron emission tomography (PET) is a functional imaging technique able to provide information on the metabolic activity in a living organism. Its principle is the detection of two 511 keV gamma rays emitted from the annihilation of a positron, generated from a β^+ decay of an isotope embedded in a drug and injected in the patient, with an electron. The gamma rays are detected in coincidence using detector blocks arranged in rings around the patient that allow recording the lines of response along which the annihilation process took place and also allow for 3D image reconstruction. To improve the signal-to-noise ratio and

therefore the overall quality of the image, the use of time-of-flight (TOF) information has become an essential tool in PET (Cherry *et al* 2006, Surti 2015).

The basic detection module is usually made of several scintillators that convert the energy of the incoming gamma into optical photons, detected by photodetectors that convert the scintillation light into an electrical signal, such as silicon photomultipliers (SiPMs). One of the most suitable scintillators for PET applications is LYSO:Ce, due to its high photon yield of 40 000 ph MeV^{-1}, high density (7.4 g cm^{-2}) and fast scintillation profile (Gundacker *et al* 2016).

To achieve high sensitivity, long scintillators are required, but they can lead to distortions in the reconstructed images due to parallax effects (Pizzichemi *et al* 2016). Moreover, as the frontier of timing is more and more pushed towards the goal of 10 ps full width at half maximum (FWHM) (Lecoq 2022), the influence of light transport on the coincidence time resolution (CTR), and its dependence on the gamma-rays' depth of interaction (DOI) along the main crystal axis, becomes no longer negligible (Gundacker *et al* 2014, Loignon-Houle *et al* 2021, Terragni *et al* 2022). The evaluation of the DOI of gamma rays along the main axis of the scintillator is fundamental to avoiding parallax errors in the image reconstruction process and achieving high spatial and timing resolution. This is of particular importance for preclinical and organ-dedicated human PET scanners that require very high spatial resolution, of the order of 1–2 mm, and that suffer from a large influence of parallax errors.

A method to effectively extract the DOI information is the use of an array of scintillators, laterally depolished and coupled on one side to a 4×4 matrix of photodetectors and on the other side to a light guide covered with a specular reflector (Pizzichemi *et al* 2016). The DOI coordinate can then be derived from the ratio of light detected by each of the SiPMs directly coupled to the scintillator and the total light collected by all the SiPMs, and as such can be used to improve the timing evaluation.

The method has been previously validated (Pizzichemi *et al* 2019) using a custom-made 32-channel board based on the NINO chip (Anghinolfi *et al* 2003). However, this custom-made readout electronics has several limitations, including a limited number of channels, high power consumption, and lack of an integrated digitalization system, which pose challenges for integrating the DOI concept into a full TOF-PET detector device. A promising alternative is the PETsys TOFPET2 ASIC (Di Francesco *et al* 2016, Bugalho *et al* 2018), a commercially available readout electronics solution that offers low power consumption and scalability to thousands of channels. This work investigates the performance of the DOI approach using the PETsys TOFPET2 ASIC with different SiPM arrays and compares the results with those obtained using the custom-made 32-channel board based on the NINO chip.

2. Materials and methods

In this section, an overview of the detector chain is presented. The configuration of the detector modules, consisting of a combination of scintillators and photodetectors, is described in section 2.1. Section 2.2 introduces the two electronic boards used in this study to read out the signals from the detectors. Lastly, section 2.3 outlines the experimental set-ups used to conduct the measurements. Two identical electronic boards are used to read out the signals from a detector module and a small reference detector ($2 \times 2 \times 3$ mm^3), used for electronic tagging, placed at opposite sides of a ^{22}Na source of 0.25 mm diameter emitting two back-to-back gamma photons in coincidence. Finally, section 2.4 addresses the module characterization.

2.1. Detector modules

Two different configurations of PET modules (Pizzichemi *et al* 2019) are used for this study (figure 1): a module with DOI capabilities, based on the use of depolished crystals and a light guide on top to enable a light-sharing scheme (DOI capable module), and a similar module making only use of polished scintillators without DOI capabilities (standard module). Both modules consist of 16 crystals of LYSO:Ce scintillators produced by Crystal Photonics Inc and an array of 4×4 SiPMs. We tested three different types of 4×4 SiPM array: (1) the S13361-3050AE-04 array from Hamamatsu, with each SiPM having an active area of 3.1×3.1 mm^2, (2) an array made of 16 NUV-HD AFBR-S4N33C013 SiPMs from Broadcom, each with a 3×3 mm^2 active area, and (3) the NUV-MT AFBR-S4N44P164M array from Broadcom, with a SiPM active area of 3.72×3.62 mm^2.

2.1.1. DOI capable module

This module consists of an LYSO package made of 16 depolished crystals, each measuring $3.1 \times 3.1 \times 15$ mm^3. Each crystal is coupled—one by one—to a single detector of the SiPM array and separated from its neighbors by foils of enhanced specular reflector (ESR) as reflective material. The side of the scintillator block opposite to the photodetectors is coupled using optical clear adhesive (OCA) of 150 μm to a 1 mm

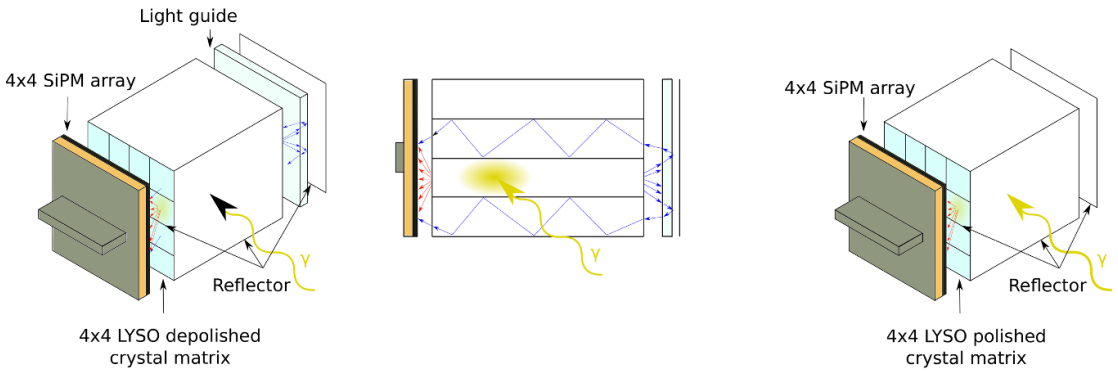

Figure 1. Structure of DOI modules (left) and standard modules (right). The two structures differ only by the presence of a light guide and the depolished surface finishing in the DOI modules.

thick glass plate to act as a light guide, thus enabling light recirculation in the neighboring crystals. Finally, a foil of ESR is placed in dry contact on the back of the light guide to act as a mirror.

The light produced in a gamma ray interaction is propagated in a pixel and emitted both from the 'photodetector-side' (red arrows in figure 1) and the opposite end 'reflector-side' (blue arrows in figure 1) and is shared with the neighboring crystals. The ratio of light emitted from the two ends of the scintillator, thanks to the optical depolishing of the lateral surfaces of the crystal, is proportional to the DOI and determines the gamma interaction point w along the crystal axis (Vilardi *et al* 2006, Trummer *et al* 2009) as

$$w = \frac{p_{\max}}{P}. \tag{1}$$

$p_{\max}$ is the maximum amount of light collected by the photodetector of the array where the interaction occurred, and

$$P = \sum_{i=1}^{K} p_i \tag{2}$$

denotes the total amount of light collected by K photodetectors. Moreover, the quantities

$$u = \frac{1}{P}\sum_{i=1}^{K} p_i x_i \ , \ \ v = \frac{1}{P}\sum_{i=1}^{K} p_i y_i \tag{3}$$

allow for the identification of the point of interaction of the gamma, making use of an Anger-logic scheme (Anger 1958).

2.1.2. Standard module

The structure of the standard module is very similar to that of the DOI module. The only differences are the use of fully polished scintillators and the absence of a light guide between the crystal matrix and the ESR foil, as shown in figure 1. As a result, light sharing is extremely reduced and no DOI capabilities are expected. On the other hand, they yield the best results in terms of timing and energy resolutions (Pizzichemi *et al* 2019).

2.1.3. SiPM arrays

Different SiPM arrays are used for this study. The Hamamatsu model S13361-3050AE-04 consists of an array of 4×4 SiPMs, each with 3.1×3.1 mm^2 active area and 50 μm single photon avalanche diode (SPAD) pitch, matching the dimensions of the crystals of the module. Moreover, an array of 16 NUV-HD SiPMs with 3×3 mm^2 active area and 30 μm SPAD pitch from Broadcom is assembled to nearly match the same dimensions of the crystal matrix. Finally, the high-performance NUV-MT (metal in trench) SiPM array from Broadcom with a total dimension of 16×16 mm^2 is tested (Merzi *et al* 2023), made of SiPMs each with a sensitive area of 3.72×3.62 mm^2 and 40 μm SPAD pitch. While the Hamamatsu and Broadcom NUV-HD arrays are equipped with Through Silicon Vias connectivity, the Broadcom NUV-MT are connected via wire bonding, which however creates non-uniform gaps between the SiPMs. The crystal modules are coupled via a 50 μm layer of OCA to the Hamamatsu 13361-3050AE-04 array and via Cargille Meltmount (refractive index $n = 1.582$) to the Broadcom arrays.

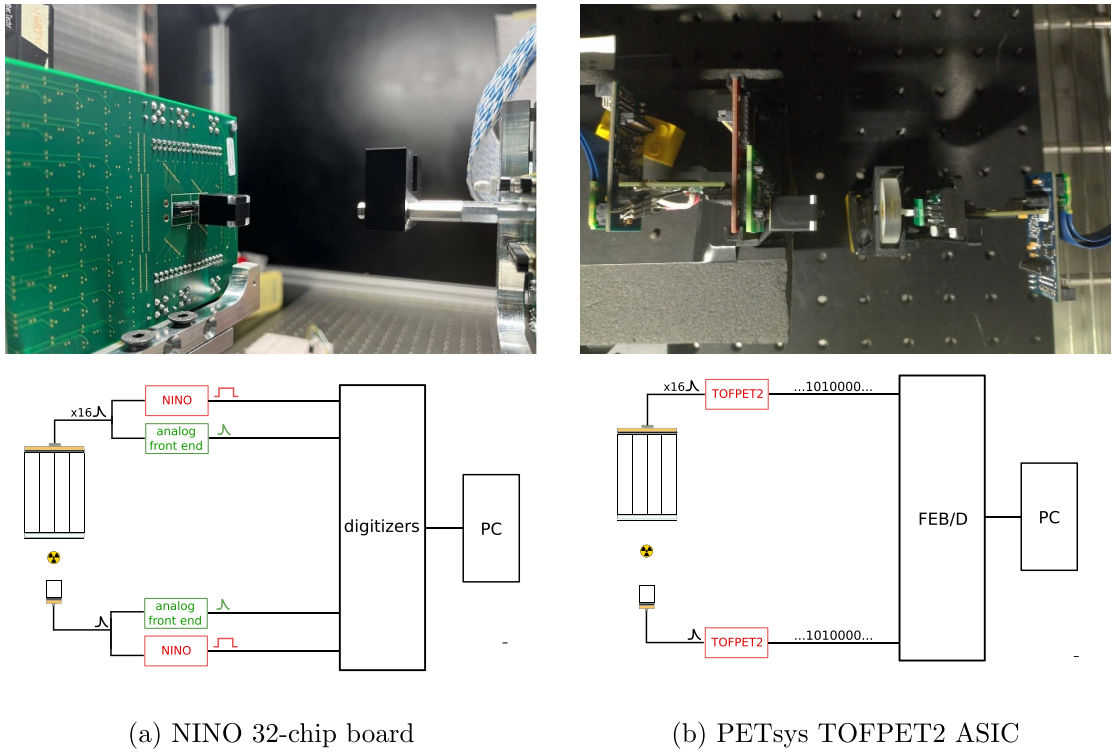

(a) NINO 32-chip board (b) PETsys TOFPET2 ASIC

Figure 2. Picture and schematics of the front end boards (FEBs) of the two set-ups used for the measurements. In particular, a DOI-capable module coupled to Hamamatsu 13361-3050AE-04 array, irradiated frontally, is shown.

2.2. Multi-channel readout electronics

To extract the DOI coordinate as described in section 2.1.1, it is essential to measure the amount of light hitting the photodetectors, and this can be done by integrating the electrical pulses generated by each of them. Simultaneously, precise timing measurements and corrections using the DOI information require a parallel multichannel readout based on fast electronics. This was already carried out using a custom-made NINO 32-chip board presented in Pizzichemi *et al* (2019), where a CTR $<$160 ps FWHM and an energy resolution $<$10% have been obtained with the described crystal modules and Hamamatsu SiPM arrays. In this work, measurements are made to evaluate the performance of Broadcom NUV-HD and NUV-MT SiPM arrays. Although promising in terms of time and energy resolutions, such a custom-made set-up is not scalable to a full system in view of its high power consumption and large dimensions.

On the other hand, the PETsys TOFPET2 ASIC, while allowing the extraction of the integrated charge and time information in a similar manner as the NINO board, is scalable to thousands of channels.

2.2.1. NINO 32-chip board

In the set-up shown in figure 2(a), an acquisition system based on two identical custom-developed front-end boards (FEBs) and a combination of CAEN VME digitizers is used (Pizzichemi *et al* 2019). Event by event, the signal generated by each photodetector is split into two components. One is amplified and fed directly to one channel of a 64ch VME V1740D CAEN module that digitizes and integrates the pulse shape. The other is routed to one input of the NINO-32 amplifier-discriminator board (Anghinolfi *et al* 2003) producing a square wave with a length analogous to the input charge (time-over-threshold (TOT) method) which is subsequently digitized by one channel of two fast 32ch VME V1742 CAEN modules (least significant bit (LSB) 200 ps). The timestamp of the event is derived from the crossing of the rising edge of this square wave over a fixed threshold. For every valid trigger, the integrated charge and the timestamp are stored for each photodetector connected to the FEBs. The value of integrated charge obtained from each SiPM is corrected for saturation effects of the SiPMs due to the finite number of SPADs present in the photodetector (Otte *et al* 2005).

2.2.2. PETsys TOFPET2 ASIC

In the second configuration shown in figure 2(b), the SiPM array is read out by the PETsys TOFPET2 ASIC (version 2c), making use of its evaluation kit from PETsys Electronics S.A.. This includes a custom sensor FEB (FEB/S) and an adapter board to connect the SiPMs, plus two FEB/A_v2 boards each with one

64-channel high-performance TOFPET2 ASIC and an interface FEB (FEB/I) connecting the ASICs to the motherboard (FEB/D_v2) via flexible Samtec high-speed coaxial (HQCD) cables. This is called the standard front-end-module (FEM-128). Two FEM-128 are used to read out two detectors in coincidence. Additional components of the evaluation kit are an HV-DAC mezzanine board generating the SiPM bias voltage and a Gigabit Ethernet (GbE) board routing data to the laboratory computer.

Each TOFPET2 ASIC is characterized by its compactness, the possibility to read out 64 channels (Nadig *et al* 2021), maximum power consumption of 8.2 mW per channel (Nadig *et al* 2019) and its high capacity of data rates of up to 600 kcps per channel. Each channel employs a three-threshold trigger logic with two discriminators D_{T1} and D_{T2} in the timing and one discriminator D_E in the energy branch (PETsys Electronics S.A. 2018a, 2018b, 2018c). The trigger circuit of each channel enables dark count rejection and high timing resolution by triggering at a low threshold with the first discriminator D_{T1}, on the first optical photons hitting the SiPM. This trigger enters an AND gate opened by a second trigger activated at a higher threshold by the second discriminator D_{T2}. A time-to-digital converter (TDC) assigns a timestamp to an event, and the energy of the respective event can then be measured either by signal integration featuring capacitors (charge-to-digital converter (QDC)-method, over a period of 290 ns) or by measuring the time over a specified threshold (tot-method). The QDC is used in QDC mode.

After calibrating the channel baselines and TDCs and QDCs, making use of the calibration routine provided with the evaluation kit software, bias and threshold scans can be performed. The thresholds of the three discriminators can be adjusted via the three dimensionless parameters vth_t1, vth_t2, and vth_e in the ASIC configuration. Increasing vth_t2, and vth_e by one digital-to-analog converter (DAC) step is equal to increasing the trigger level by approximately 15 mV and 20 mV, respectively, over a baseline determined from calibration. The second timing threshold vth_t2 = 20 and the energy threshold vth_e = 15 are kept constant, whereas the first timing threshold vth_t1 is set to the LSB value of 6.66 mV (Nadig *et al* 2022).

Using the convert_raw_to_singles_method implemented by PETsys Electronics S.A. (PETsys Electronics S.A. 2018c), raw data are converted to single hit information, each with a timestamp, energy value, and channel-ID. As previously described, the energy values are corrected to compensate for the saturation effect.

2.3. Measurements set-up

Two different set-ups are used to characterize the modules in terms of timing and DOI resolution, a front irradiation set-up, where the reference detector and source are placed in front of the detector module, and a lateral irradiation set-up, with the source and crystal placed on the side of the detector module.

2.3.1. Front irradiation

A PET-like set-up is used to run the standard characterization of the module and evaluate the time resolution. The reference detector is placed in front of the crystal matrix, i.e. opposite to the SiPM array, with the source placed in between such that the entire module is irradiated head-on as shown on the left of figure 3.

The CTR of the modules, which needs to be corrected for the CTR of the reference detector, is then derived from

$$\mathrm{CTR} = \sqrt{2 \cdot \mathrm{CTR}^2_{\mathrm{measured}} - \mathrm{CTR}^2_{\mathrm{reference}}}. \tag{4}$$

2.3.2. Lateral irradiation

To evaluate the DOI resolution, an electronic tagging configuration is used. The source and the reference detector are placed to the side of the module so as to irradiate the crystals 'laterally' (figure 3 right). The module is placed on programmable linear stages allowing to precisely align and move its position in order to establish a scan of different DOI positions along the 15 mm long axis of the crystals.

2.4. Module characterization

The *front irradiation* set-up, described in section 2.3.1, allows the characterization of each module in a two-step process: a calibration run (1) and an acquisition run (2) to assess the timing performance. The detailed description of the process can be found in Pizzichemi *et al* (2019). The calibration run is used to record the charge spectrum of the reference crystal and to remove events outside the 511 keV photopeak. For the remaining events, the calculated values of the (u, v, w) coordinates in the module are entered into a 3D and 2D plot (figure 4), where several accumulation regions can be identified and separated by means of a custom clustering algorithm (Stringhini *et al* 2016). The algorithm starts from a seed defined as the voxel with the highest number of counts C_0. It then analyses all nearby voxels, discarding the ones with a number of counts lower than a threshold C_{th}, which is defined as a fraction of C_0. The procedure is then repeated recursively for all seeds and, when no more new seeds are found, the volume associated with the complete set of seeds defines a cluster. These voxels are then removed from the 3D histogram, and the procedure starts again until 16 clusters are found.

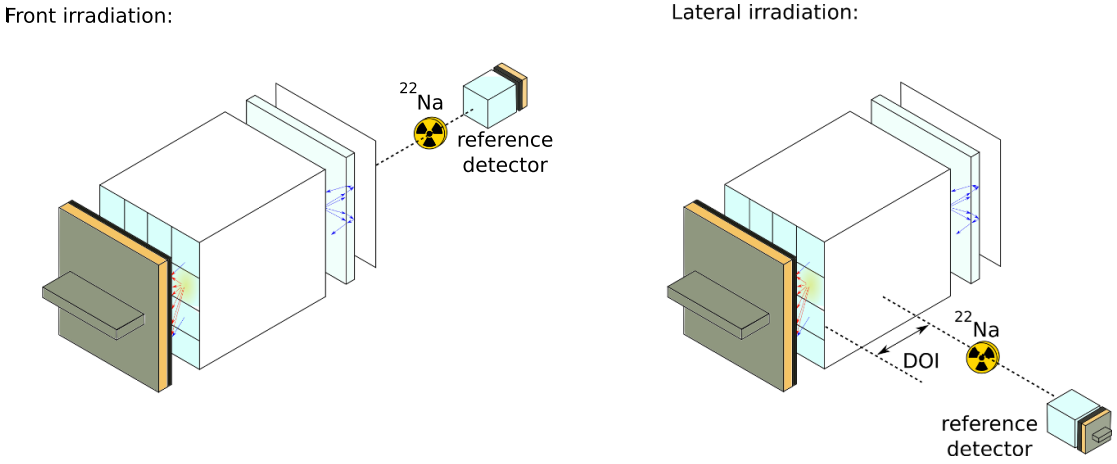

Figure 3. Front irradiation set-up used to characterize the modules in terms of time resolution (left) and lateral irradiation set-up used to evaluate the DOI resolution (right).

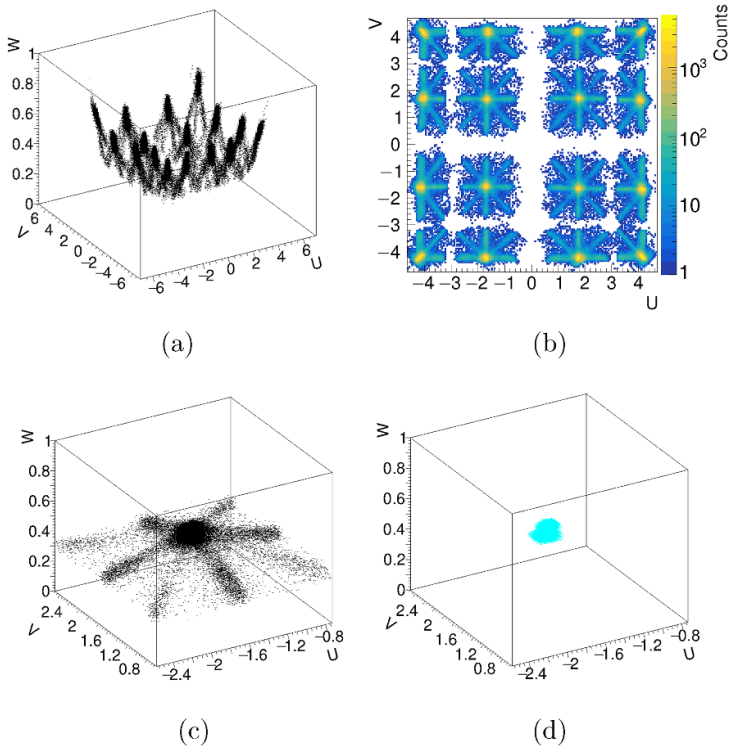

Figure 4. Identification of the gamma rays's interaction positions using the DOI-capable module, the Hamamatsu model S13361-3050AE-04 SiPM array and the NINO 32-chip board for the readout. (a) 3D and (b) 2D histograms of all events of a calibration run plotted for the DOI capable module. 16 accumulation regions can be distinguished. (c) To help visualization, the histogram is zoomed into an (u, v) area corresponding to a crystal coupled to a single SiPM. (d) Result of the clustering algorithm.

The identified volumes correspond to gamma rays interacting with individual crystals. Events whose (u, v, w) coordinates lie outside these delineated regions are interpreted as inter-crystal scatters, where a single gamma ray deposits energy in multiple crystals. For the purpose of this study, such events are excluded from the analysis. Dedicated methods can be applied to recover and make use of these events (Rafecas *et al* 2003, Gillam *et al* 2012). Using the standard module, the selected events will be confined to a region close to $w = 1$, whereas in the DOI-capable module, the region is more widely spread out and closer to $w = 0$ (as in figure 4). For each volume, the charge spectrum is reconstructed to determine the region of photopeak selection, as well as to assess the energy resolution. After selecting events within the photopeak of each individual crystal, a DOI calibration curve (figure 5(a)) can be established for each scintillator that allows the exact reconstruction of the physical gamma interaction coordinate from the w value, as described in Stringhini *et al* (2016) using the gamma attenuation function in the crystal. Then, for each detector, a 2D

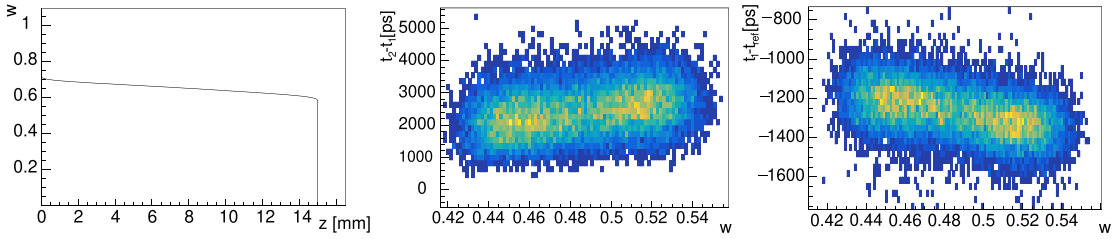

Figure 5. Front irradiation after selection of events in the accumulation volume and photopeak region of each individual crystal using the DOI-capable module, the Hamamatsu S13361-3050AE-04 SiPM array and the NINO 32-chip board for the readout. (a) Calibration curve to correctly reconstruct the physical DOI coordinate using the gamma attenuation function. (b) Scatter plot of the time delay t_i–t_1 versus w built for each detector to extract the average time delay of the ith photodetector with respect to the detector of interaction as a function of w. (c) Scatter plot of the time delay t_1–t_{ref} versus w, to derive the average delay expected as a function of w between the crystal of interaction and the external reference crystal.

histogram of the time delay (t_i–t_1) versus w is built (figure 5(b)), and the experimental relations $g_i(w) = [t_i–t_1](w)$, denoting the average delay of the i-th photodetector with respect to the detector of interaction D_1 as a function of the DOI coordinate w, are plotted for each i. Finally, another 2D scatter plot of t_1–t_{ref} versus w is produced, to derive $d(w)$, i.e. the average delay expected as a function of w between t_1 and a fixed external reference (figure 5(c)). After calibration, the acquisition run is analyzed to assess the timing performance. Only events simultaneously recorded in the photopeak of one of the crystals of the module and the reference crystal are selected. The first delay histogram H_{std} is constructed from the difference between the timestamp t_1 and t_{ref}

$$\Delta t_{std} = t_1 - t_{ref}. \tag{5}$$

The second histogram H_{corr} exploits the $d(w)$ and $g_i(w)$ functions extracted from the calibration run to correct for the DOI by using

$$\Delta t_{corr} = \hat{\Theta} - t_{ref} \tag{6}$$

with

$$\hat{\Theta} = \frac{\sum_{i=1}^{16} \left(1/\sigma^2\right) \cdot \left(t_i - g_i(w)\right)}{\sum_{i=1}^{16} \left(1/\sigma^2\right)} - \left[d(w) - d(w_0)\right]. \tag{7}$$

To extract the FWHM, the H_{std} and H_{corr} distributions are fitted using an exponentially modified Gaussian distribution and are corrected for the contribution of the reference detector as described in section 2.3.1.

Using the *lateral irradiation* set-up, described in section 2.3.2, it is possible to irradiate the matrix at known DOI positions, provided by the vertical position of the source and the reference crystal. Thus, the correlation of the DOI with the w coordinate can be studied. After applying the clustering algorithm (Stringhini *et al* 2016), the w distribution for the different vertical positions of the reference crystal is shown in figure 6(a). It is observed that, as expected, the peak position varies with z in strong correlation with the w coordinate derived from DOI information. Plotting the vertical position of the interaction versus the peak position of the w distributions a linear relation between the two variables can be established (figure 6(b))

$$\text{DOI} = m \cdot w + q. \tag{8}$$

Using this correlation to correct the peak values of each w distribution for the corresponding position in space and summing all events, the distribution of figure 6(c) is obtained. Fitting the distribution with a Gaussian function yields the crystal DOI resolution in FWHM. Repeating the process for each irradiated crystal, the DOI resolution of the module is defined as the mean value of all the extracted DOI resolutions.

Table 1 summarises the measurements performed for the described characterization of the detector modules and the SiPM arrays and electronic readouts, plus the type of irradiation configuration employed.

3. Results

Section 3.1 presents the timing performance obtained using the different SiPMs coupled to the standard module. The PETsys TOFPET2 ASIC is used for these measurements, and the results are compared with

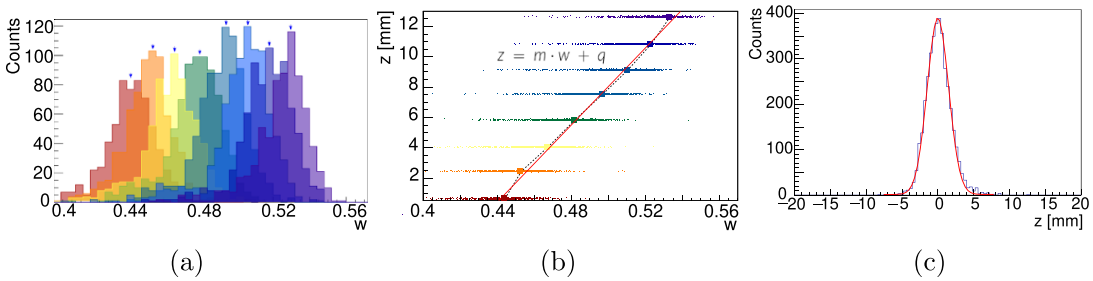

Figure 6. Lateral irradiation after application of the clustering algorithm using the DOI-capable module, the Hamamatsu S13361-3050AE-04 SiPM array and the NINO 32-chip board for the readout. (a) *w* distributions for different positions of the reference crystal along the crystal axis. (b) Linear relationship between the axial position of the interaction and the peak position of the *w* distributions. (c) Using the linear relation to correct the position of each *w* distribution and summing over all events, a Gaussian distribution is obtained. The DOI resolution is extracted as FWHM of the Gaussian fit.

Table 1. Electronic readout, crystal modules, SiPM arrays and set-up configurations investigated in this work.

Electronic readout	Crystal module	SiPM array	Irradiation
NINO 32-chip board	Standard	Hamamatsu 13361-3050AE-04	*Front*
		Broadcom NUV-HD	*Front*
		Broadcom NUV-MT	*Front*
	DOI module	Hamamatsu 13361-3050AE-04	*Front*
			Lateral
		Broadcom NUV-HD	*Front*
			Lateral
		Broadcom NUV-MT	*Front*
			Lateral
PETsys TOFPET2 ASIC	Standard	Hamamatsu 13361-3050AE-04	*Front*
		Broadcom NUV-HD	*Front*
		Broadcom NUV-MT	*Front*
	DOI module	Hamamatsu 13361-3050AE-04	*Front*
			Lateral
		Broadcom NUV-HD	*Front*
			Lateral
		Broadcom NUV-MT	*Front*
			Lateral

those obtained with the NINO 32-chip readout board. All measurements were made in front irradiation configuration. The DOI-capable module, coupled to different SiPM arrays, is laterally irradiated to examine its DOI resolution. Additionally, the DOI-capable modules are frontally irradiated to evaluate their timing resolution, similar to the standard module. The DOI correction, described in section 2.4, is also applied after the calibration procedure. Section 3.2 presents the results obtained with the DOI-capable modules for both DOI and timing capabilities. All measurement runs are summarised in table 1.

3.1. Standard module

Using the PETsys TOFPET2 ASIC, measurements are repeated varying the SiPM array overvoltage (OV) and the timing threshold vth_t1 for the different SiPM arrays. The results of the measurements are displayed in figure 7. As to the Hamamatsu SiPM array, the best timing resolution is found to be 205 $\pm$ 8 ps FWHM at OV $=$ 4 V and a threshold vth_t1 $=$ 20. A similar value of 206 $\pm$ 8 ps is obtained for the Broadcom NUV-HD array at a threshold vth_t1 $=$ 20 and OV $=$ 8 V. When utilizing the Broadcom NUV-MT array, an even better timing resolution of 193 $\pm$ 6 ps is achieved at OV $=$ 7 V and threshold vth_t1 $=$ 40. As described in section 2.2.2, to convert the threshold vth_t1 into mV, a LSB value of 6.6 mV should be used. Table 2 summarises the best results achieved with the PETsys TOFPET2 ASIC and compares them with those obtained with the NINO 32-chip board. When using the NINO 32-chip board, a CTR $=$ 141 $\pm$ 4 ps is obtained using the Broadcom NUV-MT array. No threshold scan is performed as the threshold was optimized for LYSO:Ce and the Hamamatsu array in previous studies (Pizzichemi *et al* 2019).

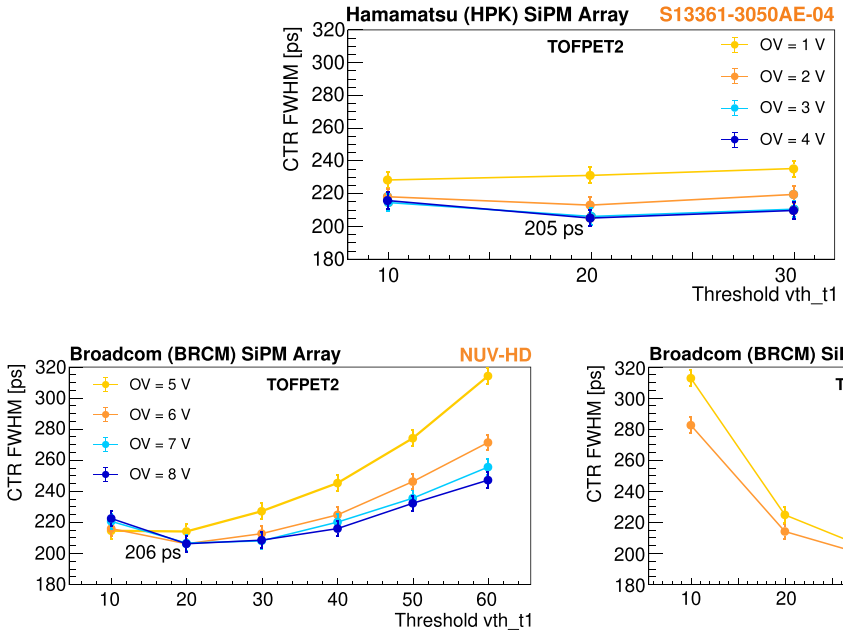

Figure 7. CTR results using the standard module and PETsys TOFPET2 ASIC in front irradiation configuration are shown. (Top) Results using the Hamamatsu SiPM array. (Bottom) Broadcom NUV-HD and NUV-MT.

Table 2. CTR results using the standard module, coupled to different SiPM types from Hamamatsu and Broadcom with PETsys TOFPET2 ASIC and NINO 32-chip board readout in front irradiation configuration. To convert the threshold vth_t1 into mV, a LSB value of 6.6 mV should be used. The Hamamatsu SiPM type is 13 361-3050AE-04.

Electronic readout	SiPM array	OV (V)	Threshold	CTR FWHM (ps)
PETsys TOFPET2 ASIC	Hamamatsu	4 V	20	205 ± 8 ps
	Broadcom NUV-HD	7 V	20	206 ± 6 ps
	Broadcom NUV-MT	9 V	40	193 ± 6 ps
NINO 32-chip board	Hamamatsu[a]	7 V[a]	—	162 ± 2 ps[a]
	Broadcom NUV-HD	4 V	—	166 ± 5 ps
	Broadcom NUV-MT	9 V	—	141 ± 4 ps

[a] Values from Pizzichemi *et al* (2019).

Table 3. DOI results with the DOI capable module, coupled to different SiPM types from Hamamatsu and Broadcom, and read out with PETsys TOFPET2 ASIC and the NINO 32-chip board in lateral irradiation configuration.

Electronic readout	SiPM array	OV (V)	DOI FWHM (mm)
PETsys TOFPET2 ASIC	Hamamatsu 13361-3050AE-04	4 V	3.5 ± 0.3 mm
	Broadcom NUV-HD	7 V	2.9 ± 0.4 mm
	Broadcom NUV-MT	9 V	2.6 ± 0.2 mm
NINO 32-chip board	Hamamatsu 13361-3050AE-04[a]	7 V[a]	3.1 ± 0.1 mm[a]
	Broadcom NUV-HD	4 V	3.2 ± 0.1 mm
	Broadcom NUV-MT	9 V	2.5 ± 0.2 mm

[a] Values from Pizzichemi *et al* (2019).

3.2. DOI module

3.2.1. DOI evaluation

The reference detector is positioned on the side of the detector array at a distance that ensures the irradiation of a spot with a maximum diameter of 1 mm. The measurement is made using the optimal SiPM bias voltage already determined from the measurements of the standard module. The DOI resolution is evaluated as in section 2.4. The results obtained using the Hamamatsu and Broadcom arrays are summarized in table 3.

3.2.2. CTR evaluation

The reference detector is positioned again in front of the detector array, with the source placed in between and close to the reference detector to ensure that the entire crystal matrix is irradiated. Using the PETsys

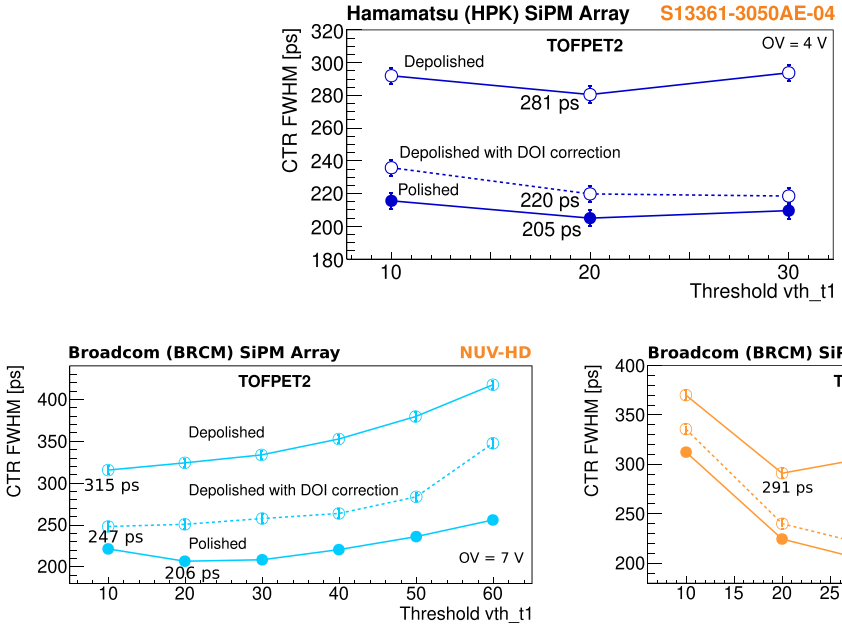

Figure 8. CTR results using the DOI module and PETsys TOFPET2 ASIC in front irradiation configuration. (Top) Results using the Hamamatsu SiPM array. (Bottom) Broadcom NUV-HD and NUV-MT.

Table 4. CTR results using the DOI module, coupled to different SiPM types from Hamamatsu and Broadcom and readout using PETsys TOFPET2 ASIC and the NINO 32-chip board in front irradiation configuration. The results of the standard module at the same SiPM array OV are also shown for comparison. The Hamamatsu SiPM type is 13 361-3050AE-04.

		DOI module		std module
Electronic readout	SiPM array	CTR_{std}	CTR_{corr}	CTR_{std}
PETsys TOFPET2 ASIC	Hamamatsu	281 ± 8 ps	224 ± 8 ps	205 ± 8 ps
	Broadcom NUV-HD	315 ± 7 ps	247 ± 7 ps	206 ± 6 ps
	Broadcom NUV-MT	291 ± 6 ps	216 ± 6 ps	193 ± 6 ps
NINO 32-chip board	Hamamatsu[a]	233 ± 2 ps[a]	165 ± 2 ps[a]	162 ± 2 ps[a]
	Broadcom NUV-HD	253 ± 8 ps	179 ± 6 ps	166 ± 5 ps
	Broadcom NUV-MT	247 ± 7 ps	170 ± 5 ps	141 ± 4 ps

[a] Values from Pizzichemi *et al* (2019).

TOFPET2 ASIC, measurements are repeated varying the threshold vth_t1 at the optimal OV found for the different SiPM arrays and the standard module. The results of the measurements are shown in figure 8, comparing the CTR extracted before and after DOI correction. The optimal values are summarized in table 4.

4. Discussion

Tables 3 and 4 summarize the results obtained in terms of CTR and DOI resolution.

Using the standard module, a clear improvement is obtained with the NUV-MT SiPM from Broadcom, which achieves a CTR of 141 ± 4 ps with the custom-made NINO 32-chip board and 193 ± 6 ps with the PETsys TOFPET2 ASIC. Although the custom-made NINO 32-chip board shows higher performance, it is not scalable to a full system, due to the limitation to 32 channels, higher power consumption (27 mW/channel (Anghinolfi *et al* 2003)), and missing integration of a TDC and QDC system. On the other hand, the PETsys TOFPET2 ASIC demonstrates the feasibility of building modules using commercially available crystals and SiPMs, with a timing resolution better than 200 ps FWHM. In its present form, the modules can be scaled up from sixteen to hundreds of channels without adding hardware complexity to the detector and ASIC development. However, increasing the number of channels would introduce particular complexity to the data analysis framework, and this will be the subject of future work. In fact, by measuring coincidences between two module prototypes, rather than between one module and the reference, the number of potential coincidences between channels would increase from 16 to 16^2. This number grows quadratically with the number of channels.

To build a high-resolution PET scanner targeted for small animals or specific organs in the human body, the ability to extract the information on the DOI becomes essential to correct for the parallax error. The DOI-capable modules using the Hamamatsu SiPM array and PETsys TOFPET2 ASIC have shown a DOI resolution of 3.5 ± 0.3 mm, in agreement with Stringhini *et al* (2016) and Pizzichemi *et al* (2016), who already in 2016 demonstrated a DOI resolution of ∼3 mm using the NINO 32-chip board. The resolution slightly improves when using the SiPMs with the newly developed metal in trench technology by Broadcom and Fondazione Bruno Kessler (Merzi *et al* 2023). This technology reduces the internal optical crosstalk, resulting in lower dark current and allowing for higher OVs to be achieved. Despite the initial degradation in time performance from the depolishing of the crystal surfaces and the light-sharing, the time resolution is partially recovered owing to the use of the DOI information. The best result, once again, is obtained using the Broadcom NUV-MT array. Nevertheless, the CTR still remains worse compared to that of the standard module. This can be attributed to several factors. First, the geometry of the crystal matrix allows a perfect 1:1 matching of crystals and SiPMs exclusively for the Hamamatsu SiPM array (3.1×3.1 mm^2), in contrast to the Broadcom NUV-HD and NUV-MT arrays, where each SiPM active area measures 3×3 mm^2 and 3.72×3.62 mm^2, respectively. While perfect matching is not required in the case of a polished crystal matrix, it is important for DOI-capable structures because they are prone to correlations due to light detected by neighboring SiPMs. Moreover, if one uses Cargille Meltmount instead of OCA for the coupling of the crystal matrices to the SiPM arrays, as in the case of the Broadcom arrays, there is the possibility that the compound penetrates over time between the crystals. This increases front light sharing and thereby the dependency on the DOI in the crystal region near the SiPM is partially lost. Simulations show that this effect could be mitigated if one used very thin layers of coupling compounds between the crystal matrix and the SiPMs. This should lead to visible improvements both in terms of DOI and time resolutions, and this will also be subject to future work. Once this condition is met, the DOI-capable module would not only achieve the same time resolution of the standard module (Pizzichemi *et al* 2019) but also provide sub 3 mm DOI resolution, without increasing hardware complexity or cost.

5. Conclusions

We have investigated the performance of a DOI-capable module with a length of 15 mm based on a light-sharing principle using the commercially available PETsys TOFPET2 ASIC and several SiPM arrays from Hamamatsu and Broadcom. The NUV-MT arrays demonstrated the best performance in terms of timing and DOI resolution. Using a Broadcom NUV-MT SiPM array, the module achieved timing and DOI resolutions of 216 ± 6 ps FWHM and 2.6 ± 0.2 mm FWHM, respectively. Results are compared to those obtained with a custom-made NINO 32-chip board. While the CTR is better than that obtained with the TOFPET2 ASIC, the set-up based on the PETsys TOFPET2 ASIC has the advantage of being suitable for large-scale applications in preclinical or clinical PET detectors. The light-sharing scheme allows efficient extraction of the DOI information with high resolution, partially compensating for the loss in CTR. Finally, using the NUV-MT arrays and PETsys TOFPET2 ASIC with the standard module, a CTR as good as 193 ± 6 ps FWHM is achieved. Future research will focus on optimizing the crystal geometry to ensure proper coupling of the crystal matrix to the SiPM array, with the goal of improving the CTR of the DOI-capable module, which already showed excellent DOI resolution, towards that of the standard module. Additionally, different crystal lengths, particularly 20 mm, as this is the typical length used in commercial scanners, will be tested. Another direction of research will explore utilizing this detector concept to evaluate Compton kinematics in inter-crystal scatter events. This could allow for the recovery of these events and further increase the sensitivity of the detector prototype.

Data availability statement

The data cannot be made publicly available upon publication because no suitable repository exists for hosting data in this field of study. The data that support the findings of this study are available upon reasonable request from the authors.

Acknowledgments

This work is carried out in the framework of the Crystal Clear Collaboration. It is supported by the CERN Austrian Doctoral Student Programme, CERN Budget for Knowledge Transfer to Medical Applications, and the START Program of the Faculty of Medicine of RWTH Aachen University. The authors would like to disclose the following conflict of interest: Volkmar Schulz is a co-founder of Hyperion Hybrid Imaging Systems GmbH.

ORCID iDs

Giulia Terragni https://orcid.org/0000-0002-1030-0758
Vanessa Nadig https://orcid.org/0000-0002-1566-0568
Stefano di Gangi https://orcid.org/0009-0002-3685-1459
Thomas Meyer https://orcid.org/0009-0003-1064-0060
Johann Marton https://orcid.org/0000-0001-5139-7720
Stefan Gundacker https://orcid.org/0000-0003-2087-3266
Marco Pizzichemi https://orcid.org/0000-0001-5189-230X
Etiennette Auffray https://orcid.org/0000-0001-8540-1097

References

Anger H O 1958 Scintillation camera *Rev. Sci. Instrum.* **29** 27–33
Anghinolfi F, Jarron P, Krummenacher F, Usenko E and Williams M 2003 Nino, an ultra-fast, low-power, front-end amplifier discriminator for the time-of-flight detector in alice experiment *2003 IEEE Nuclear Science Symp.. Conf. Record (IEEE Cat. No. 03CH37515)* vol 1 (IEEE) pp 375–9
Bugalho R *et al* 2018 Experimental results with TOFPET2 ASIC for time-of-flight applications *Nucl. Instrum. Methods Phys. Res.* A **912** 195–8
Cherry S R, Dahlbom M and Dahlbom M 2006 *PET: Physics, Instrumentation and Scanners* (Springer)
Di Francesco A, Bugalho R, Oliveira L, Pacher L, Rivetti A, Rolo M, Silva J, Silva R and Varela J 2016 TOFPET2: a high-performance ASIC for time and amplitude measurements of SiPM signals in time-of-flight applications *J. Instrum.* **11** C03042
Gillam J E, Solevi P, Oliver J F and Rafecas M 2012 Inclusion of inter crystal scatter data in PET *2012 9th IEEE Int. Symp. on Biomedical Imaging (ISBI)* (IEEE) pp 62–65
Gundacker S, Auffray E, Pauwels K and Lecoq P 2016 Measurement of intrinsic rise times for various L(Y)SO and LuAG scintillators with a general study of prompt photons to achieve 10 ps in TOF-PET *Phys. Med. Biol.* **61** 2802
Gundacker S, Knapitsch A, Auffray E, Jarron P, Meyer T and Lecoq P 2014 Time resolution deterioration with increasing crystal length in a TOF-PET system *Nucl. Instrum. Methods Phys. Res.* A **737** 92–100
Lecoq P 2022 On the way to the 10 ps time-of-flight pet challenge *Eur. Phys. J. Plus* **137** 1–7
Loignon-Houle F, Gundacker S, Toussaint M, Lemyre F C, Auffray E, Fontaine R, Charlebois S A, Lecoq P and Lecomte R 2021 DOI estimation through signal arrival time distribution: a theoretical description including proof of concept measurements *Phys. Med. Biol.* **66** 095015
Merzi S, Brunner S E, Gola A, Inglese A, Mazzi A, Paternoster G, Penna M, Piemonte C and Ruzzarin M 2023 NUV-HD SiPMs with metal-filled trenches *J. Instrum.* **18** 05040
Nadig V, Schug D, Weissler B and Schulz V 2021 Evaluation of the PETsys TOFPET2 ASIC in multi-channel coincidence experiments *EJNMMI Phys.* **8** 1–21
Nadig V, Weissler B, Radermacher H, Schulz V and Schug D 2019 Investigation of the power consumption of the petsys TOFPET2 ASIC *IEEE Trans. Radiat. Plasma Med. Sci.* **4** 378–88
Nadig V, Yusopova M, Radermacher H, Schug D, Weissler B, Schulz V and Gundacker S 2022 A comprehensive study on the timing limits of the TOFPET2 ASIC and on approaches for improvements *IEEE Trans. Radiat. Plasma Med. Sci.* **6** 893–903
Otte A N, Barral J, Dolgoshein B, Hose J, Klemin S, Lorenz E, Mirzoyan R, Popova E and Teshima M 2005 A test of silicon photomultipliers as readout for PET *Nucl. Instrum. Methods Phys. Res.* A **545** 705–15
PETsys Electronics S.A. 2018a *TOFPET 2 SiPM Readout ASIC (rev.2)* (available at: www.petsyselectronics.com/)
PETsys Electronics S.A. 2018b *TOFPET2 ASIC Evaluation Kit—Hardware User Guide (v1.2)* (available at: www.petsyselectronics.com/) (Accessed May 2018)
PETsys Electronics S.A. 2018c *TOFPET2 ASIC Evaluation Kit—Software User Guide V2018.04* (available at: www.petsyselectronics.com/) (Accessed April 2018)
Pizzichemi M, Polesel A, Stringhini G, Gundacker S, Lecoq P, Tavernier S, Paganoni M and Auffray E 2019 On light sharing TOF-PET modules with depth of interaction and 157 ps FWHM coincidence time resolution *Phys. Med. Biol.* **64** 155008
Pizzichemi M, Stringhini G, Niknejad T, Liu Z, Lecoq P, Tavernier S, Varela J, Paganoni M and Auffray E 2016 A new method for depth of interaction determination in PET detectors *Phys. Med. Biol.* **61** 4679
Rafecas M, Böning G, Pichler B, Lorenz E, Schwaiger M and Ziegler S 2003 Inter-crystal scatter in a dual layer, high resolution LSO-APD positron emission tomograph *Phys. Med. Biol.* **48** 821
Stringhini G, Pizzichemi M, Ghezzi A, Stojkovic A, Paganoni M and Auffray E 2016 Development and evaluation of a practical method to measure the depth of interaction function for a single side readout PET detector *J. Instrum.* **11** 11014
Surti S 2015 Update on time-of-flight PET imaging *J. Nucl. Med.* **56** 98–105
Terragni G, Pizzichemi M, Roncali E, Cherry S R, Glodo J, Shah K, Ariño-Estrada G, Auffray E, Ghezzi A and Kratochwil N 2022 Time resolution studies of thallium based Cherenkov semiconductors *Front. Phys.* **10** 93
Trummer J, Auffray E and Lecoq P 2009 Depth of interaction resolution of LuAP and LYSO crystals *Nucl. Instrum. Methods Phys. Res.* A **599** 264–9
Vilardi I *et al* 2006 Optimization of the effective light attenuation length of YAP:Ce and LYSO:Ce crystals for a novel geometrical PET concept *Nucl. Instrum. Methods Phys. Res.* A **564** 506–14